Assessment of Accrued Damage and Remaining Useful Life in Leadfree Electronics Subjected to Multiple Thermal Environments of Thermal Aging and Thermal Cycling

Pradeep Lall, *Fellow, IEEE*, Rahul Vaidya, Vikrant More, and Kai Goebel

Abstract—Electronic systems are often stored for long periods prior to deployment in the intended environment. Aging has been previously shown to effect the reliability and constitutive behavior of second-level leadfree interconnects. Deployed systems may be subjected to cyclic thermo-mechanical loads subsequent to deployment. Prognostication of accrued damage and assessment of residual life is extremely critical for ultrahigh reliability systems in which the cost of failure is too high. The presented methodology uses leading indicators of failure based on microstructural evolution of damage to identify impending failure in electronic systems subjected to sequential stresses of thermal aging and thermal cycling. The methodology has been demonstrated on area-array ball-grid array test assemblies with Sn3Ag0.5Cu interconnects subjected to thermal aging at 125 °C and thermal cycling from −55 to 125 °C for various lengths of time and cycles. Damage equivalency methodologies have been developed to map damage accrued in thermal aging to the reduction in thermo-mechanical cyclic life based on damage proxies. Assemblies have been prognosticated to assess the error with interrogation of system state and assessment of residual life. Prognostic metrics including $\alpha - \lambda$ metric, sample standard deviation, mean square error, mean absolute percentage error, average bias, relative accuracy (RA), and cumulative RA have been used to compare the performance of the damage proxies.

Index Terms—Failure mechanisms, health management, leadfree solders, prognostics, reliability, remaining useful life, thermo-mechanics.

I. INTRODUCTION

THE ability to predict failures in systems and their sub-components has potential to mitigate the risks of unanticipated failures and reduce the support costs. Prognostic methods which assess system health status and predict system degradation before an actual failure occurs are needed for electronics to avoid catastrophic failure and system shutdown. Prognostic health monitoring of electronics has extreme relevance in high reliability applications to determine the current state of health of a system, identify faults, their progression, and assess accumulated damage and provide estimates of remaining life of the product. Maintenance has evolved over the years from corrective maintenance to performing time-based preventive maintenance. Future improvements in reduction of system downtime require emphasis on early detection of degradation mechanisms. Incentive for development of prognostics and health management methodologies has been provided by need for reduction in operation and maintenance process costs [1]–[3].

Avionics systems require ultrahigh reliability to fulfill critical roles in autonomous aircraft control and navigation, flight path prediction and tracking, and self-separation. Complex electrical power systems (EPS) which broadly comprise of energy generation, energy storage, power distribution, and power management, have a major impact on the operational availability, and reliability of avionic systems. Technology trends in evolution of avionics systems point toward more electric aircraft and the prevalent use of power semiconductor devices in future aircraft and space platforms. Advanced health management techniques for EPS and avionic systems are required to meet the safety, reliability, maintainability, and supportability requirements of aeronautics and space systems. Current health management techniques in EPS and avionic systems provide very-limited or no-visibility into health of power electronics, and packaging to predict impending failures [4]–[7]. Electronics systems may be subjected to prolonged periods of thermal exposure over wide temperature extremes and long periods of thermal aging at often high ambient temperatures. High-real systems may have very long operating life times with low downtime during operation. Historical environmental conditions to which the systems may have been subjected may be often unavailable. Prognostic health management (PHM) for electronics has wide applicability spanning a number of different areas. Electronics used in critical applications like space, military and avionics require multiple deployments with sequential thermal stresses. Systems may also be subjected to long term dormant storage in uncontrolled thermal environments. Ultrahigh reliability is needed to ensure predictable operation when needed and avoid any catastrophic damage during the service life.

Previously, [8]–[34] has developed leading indicators based prognostic and health management methodologies for residual life computation of electronics subjected to single, multi-
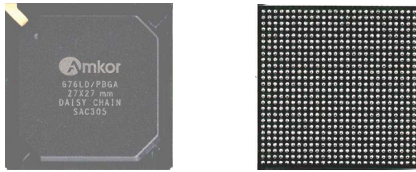
Fig. 1.   Plastic ball grid array (PBGA) 676 packages.

Fig. 2.   Test assembly design.

TABLE I
PACKAGE ARCHITECTURE DETAILS FOR TEST VEHICLE

Solder	Sn3Ag0.5Cu
Package size (mm)	27 × 27
Package type	PBGA
I/O count	676
I/O pitch (mm)	1
Ball diameter (mm)	0.63
Mold thickness (mm)	1.17
Die size (mm)	25 × 25
Substrate pad	SMD
Board finish	ImAg
Test condition	Thermal aging at 125 °C Thermal cycling −55 °C to 125 °C

ple and superimposed thermal environments comprising of isothermal aging and thermal cycling. Examples of damage pre-cursors include micro-structural evolution of second-level solder interconnects, inter-metallic compound growth, stress and stress gradients. Pre-cursors have been developed for both eutectic 63Sn37Pb and various leadfree alloy compositions like Sn4Ag0.5Cu, Sn3Ag0.5Cu, Sn1Ag0.5Cu, Sn0.3Ag0.7Cu, Sn3Ag0.5Cu-Bi, Sn3Ag0.5Cu-Bi-Ni, 96.5Sn3.5Ag alloy systems on a variety of area-array architectures. Researchers have reported the detrimental effect of thermal aging on the mechanical behavior of leadfree solders used in second-level interconnects of component level packaging. It has been shown that the degradation of the mechanical and creep properties of the solders during aging is caused due to the micro-structural evolution. The aging effects are significant even at room temperature [35]. In electronics assemblies, the built-in-self test (BIST) circuit involving error detection and correction circuits are used to give electronic assemblies the ability to test and diagnose themselves with minimal interaction from external test equipment [36]–[40]. The results obtained from BIST functions can generate diagnostic information which in turn provides additional confidence in the measurement result and confirms the device availability. BIST helps in minimizing the interaction with external automated test equipment as well as provides the advantage of a more robust "at-speed" test of the circuitry; however, the current form of BIST gives little insight about the system level reliability or the remaining useful life (RUL) of the system. Several studies conducted [37], [41]–[43] have shown that BIST can be prone to false alarms and can result in unnecessary costly replacement, re-qualification, delayed shipping, and loss of system availability. Fuses and Canaries may be mounted on a part to provide advance warning of failure due to specific wear out failure mechanism. Advanced warning is used to provide a maintenance-window for correction action, after an initial failure or malfunction, to prevent additional or secondary failures [44], [45]. Current PHM application areas include, fatigue crack damage in mechanical structures such as those in aircraft [46], surface ships [47], civil infrastructure [48], motors [49]–[51], hybrid electric vehicles [52], hydraulic actuator [53], railway structures [54], and power plants [1]. However, past efforts have provided limited insight into methods for estimation of RUL.

There is need for tools and techniques which will enable the spot-assessment of the system's health and provide method for estimation of RUL. Prognostication of sequential thermomechanical damage under thermal aging and thermal cycling based on damage pre-cursors is currently beyond the state-of-art. In this paper, a PHM method has been developed
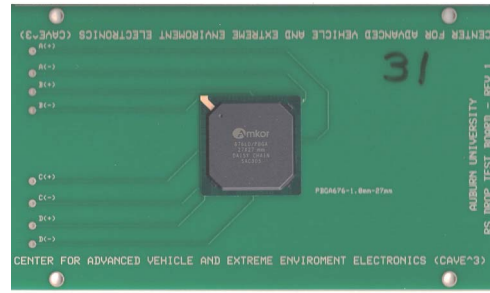
for the interrogation of system state and the estimation of RUL of systems subjected to sequential stresses. Data on damage pre-cursors have been collected and analyzed for both aging and cycling to develop a technique that can map aging time into number of cycles and thus account for reduction in life due to dormant storage. The methodology involves the use of condition monitoring devices which have been interrogated for aging, cycling, and different combinations of aging and cycling for residual life predictions. Developed PHM technique is based on non-linear least-squares method called Levenberg–Marquardt (LM) algorithm which has been developed for two different damage proxies. Prognostic model performance based on standard prognostic metrics has also been evaluated for both the damage proxies to determine which leading indicator of failure can be employed for accurate life prediction. Results of interrogation of system state have been compared with a second set of experimental-matrix to validate the proposed methodology.

II. TEST-VEHICLE

In this paper, leadfree assemblies with 676-ball PBGA676 packages were used. The packages were full-array configuration and Sn3Ag0.5Cu solder interconnects at 1 mm pitch. The ball diameter is 0.63 mm and the die size is 25 × 25 mm. Package attributes are shown in Table I. The printed circuit board was a double-sided FR4-06 material. The printed circuit board pads were solder mask defined (SMD) with immersion solver finish. Fig. 1 shows the PBGA676 package and its array configuration. A typical assembly is shown in Fig. 2. All test vehicles were subjected to sequential environments of
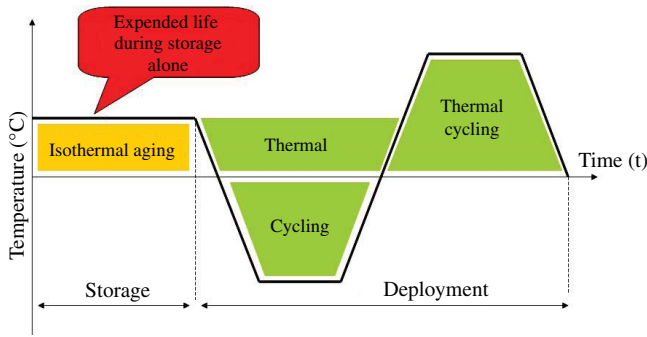
Fig. 3. Exposure of electronics to sequential stresses of thermal-aging and cycling.

Fig. 4. Micrograph and gray scale mapping of image using image analysis software.

thermal aging at 125 °C and thermal cycling from −55 °C to 125 °C for various lengths of time. The test board is a Joint Electron Devices Engineering Council form-factor test board with corner holes. Each test package has four daisy chain patterns corresponding to the four quadrants. Packages were assembled at in-house surface mount facility of CAVE[3].

III. APPROACH FOR PROGNOSTICATION OF DAMAGE IN SEQUENTIAL THERMAL AGING AND THERMAL CYCLING

In operational environments, electronic systems may be stored after manufacture for a finite period prior to deployment. During the storage period, the systems may be exposed to period of thermal aging at room temperature or at an elevated temperature. Once deployed, the systems may be exposed to thermo-mechanical cycling (Fig. 3). Extended exposure to thermal aging may reduce thermo-mechanical reliability in cyclic environments. A framework has been developed to account for the damage incurred due to storage before the deployment to determine the operational readiness of the system and compute RUL in the intended field. In thermal cyclic environments, system-life is often measured in number of thermal cycles. However, life in thermal aging environment be measured in terms of time i.e., number of hours, days, weeks or months. Assessment of cumulative damage after exposure to multiple environments is often challenging because of the differing measurement scales and scarcity of methods for reconciling damage accrued under various environmental loads. In this paper, a damage equivalency method has been presented based on the underlying failure physics to relate the damage accrued under steady-state thermal aging and cyclic thermal environments. Test assemblies were subjected to single and sequential environments of thermal aging at 125 °C and thermal cycling from −55 °C to 125 °C for various lengths of time. The approach has been developed in three steps.

A. Micro-Structural Evolution of Damage Under Single Stresses

In this step, board assemblies have been subjected to single stresses of thermal aging and thermal cycling. Samples have been withdrawn periodically and cross-sectioned. Damage proxies studied include the phase-growth parameter
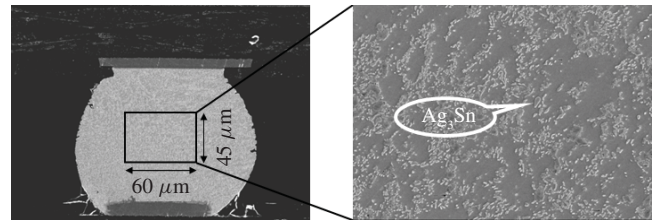
and the intermetallic (IMC) thickness. Previously, it has been shown that the rate of change in phase growth parameter [d(lnS)/d(lnN)] is valid damage proxy for prognostication of thermo-mechanical damage in solder interconnects and assessment of residual life [12]–[14], [18]–[24]. The damage proxy [d(lnS)/d(lnN)] is related to the microstructural evolution of damage by the following equation:

$$S = g^4 - g_0^4 = a (N)^b \tag{1}$$

$$\ln S = \ln \left(g^4 - g_0^4 \right) = \ln a + b \ln N$$

$$\frac{d (\ln S)}{d (\ln N)} = b \tag{2}$$

where, g is the average grain size at time of prognostication, g_0 is the average grain size of solder after reflow, N is the number of thermal cycles, S is the phase growth parameter, parameters a and b are the coefficient and exponent, respectively. The phase growth parameter, S, is the difference between the fourth-power of the phase-size at the present time and the phase-size in the pristine part, and is represented by (1). The log-plot of the equation provides a straight line relationship between the phase growth parameter and the number of cycles. It is anticipated that the higher temperature cycle magnitude will result in more accrued thermo-mechanical damage and a higher slope of the phase growth parameter versus number of thermal cycle curve. Cross-sectioned/polished samples were then gold sputter coated so as to take scanning electron microscope (SEM) images at 750 × magnification. Growth rate of tin and Ag_3Sn phases was measured. Phase size is measured using SEM and image analysis. The quantitative measure of Ag_3Sn phase size was determined from a 60 μm × 45 μm rectangular region selected from a backscattered SEM image of a highest strain solder interconnect. The images were mapped to black-and-white from gray scale image to calculate the average phase size for selected region. Fig. 4 shows the mapping of image.

Growth of IMC thickness during thermal aging has been studied as another leading indicator of failure in bulk solder. From past studies, it has been established that growth of IMC thickness is used as a damage precursor for computation of RUL [12], [13], [18]–[24]. The interfacial IMC layers are formed between solder and copper, and some precipitates appear near the interface of the IMCs/solder. These IMC layers have been identified in SEM micrographs to consist of Cu_3Sn and Cu_6Sn_5 phases [13]. In order to investigate the correlation of interfacial IMC thickness growth versus thermal aging and thermal cycling, components have been withdrawn
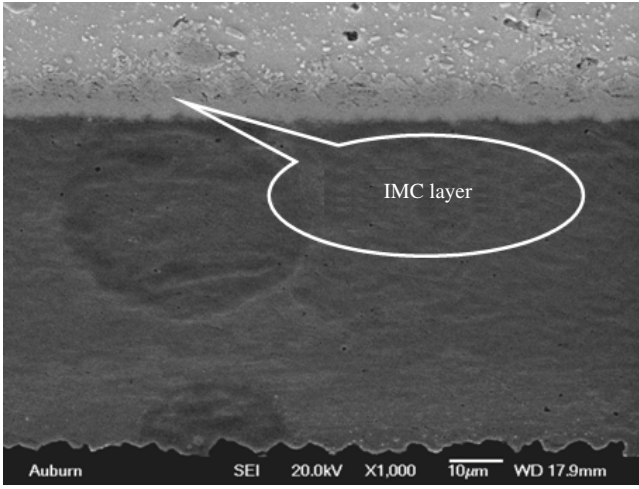
Fig. 5. SEM back-scattered images of IMC growth at 125 °C (magnification 1000×).

Fig. 6. Concept of damage equivalency and mapping of life consumed due to storage.

and cross sectioned at various intervals of thermal aging. The aged components were cross-sectioned periodically to measure the IMC thickness in SEM using 1000× magnification. The mean thickness of IMC layers was measured using commercial image processing software on SEM images, as a shown in Fig. 5. Trend analysis of IMC thickness growth on SEM using image processing software, indicates a square root dependence of IMC thickness versus aging time

$$y = y_0 + kt^n \qquad (3)$$

where $y(t)$ is IMC growth thickness during aging, y_0 is the initial thickness of IMC compounds, k is the coefficient standing for the square root of the diffusivity at aging temperature, and t is test time. The growth of IMC often follows Fick's law [55]–[58]. The exponent value, $n = 1/2$ has been used in the above equation, which reveals a diffusion-controlled mechanism during aging. Previous studies by the authors have focused on prognostication of damage under single stresses. In this paper, a method for prognosticating damage in systems subjected to sequential steady-state thermal and cyclic thermo-mechanical stresses has been developed. Damage equivalency relationships have been developed between damage accrued under thermal stresses and cyclic thermo-mechanical stresses.

B. Damage Equivalency Relationships for Thermal Aging and Thermal Cycling

A combined plot for thermal-aging and thermal-cycling in terms of damage accrual proxy and life in terms of number of cycles is shown in Fig. 6. For overlapping stresses of thermal aging and thermal cycling, the phase-growth damage proxy has been normalized as follows:

$$S_{N\Delta T} = \left(\frac{g_p}{g_0}\right)^4 - 1 = a_{n\Delta T} (N)^{b_{n\Delta T}} \qquad (4)$$

where g is the phase-growth, subscripts p and 0 indicate point "p" and initial time, respectively, $S_{N\Delta T}$ is the normalized phase-growth parameter during thermal cycling, $a_{n\Delta T}$
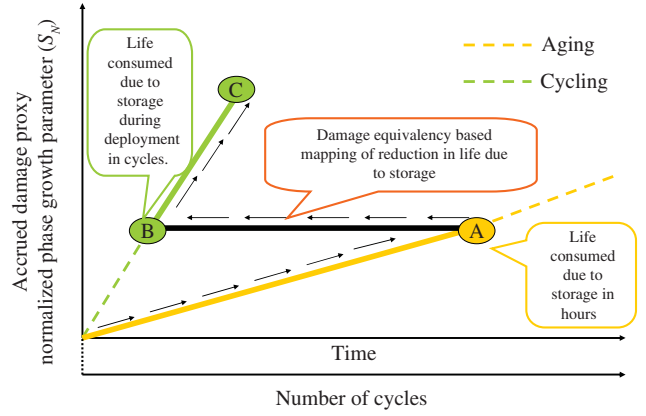
and $b_{n\Delta T}$ are the normalized phase-growth coefficient and phase growth exponent during thermal cycling. The normalized equation has been used for developing damage equivalency relations between damage accrued in thermal aging and thermal cycling. Phase-coarsening will also occur during thermal aging also. Micro-structural evolution in thermal aging can be represented as follows:

$$S_{Nt} = \left(\frac{g_p}{g_0}\right)^4 - 1 = a_{nt} (t)^{b_{nt}} \qquad (5)$$

where, g is the phase-growth, subscripts p and 0 indicate point "p" and initial time, respectively, S_{Nt} is the normalized phase-growth parameter during thermal aging, a_{nt} and b_{nt} are the normalized phase-growth coefficient and phase growth exponent for thermal aging. Since the same value of normalized phase coarsening can be achieved on in either thermal aging or thermal cycling, damage equivalency relationship has been derived by equating the normalized phase-growth parameter:

$$a_{n\Delta T} (N)^{b_{n\Delta T}} = a_{nt} (t)^{b_{nt}} \qquad (6)$$

$$N = \left[\left(\frac{a_{nt}}{a_{n\Delta T}}\right) (t)^{b_{nt}}\right]^{\frac{1}{b_{n\Delta T}}}. \qquad (7)$$

Fig. 6 illustrates the solution for damage equivalency at point A and B in thermal cycling and thermal aging, respectively. In an operational component, the accrued damage in thermal aging will result in reduction in the thermo-mechanical fatigue life of the component. The normalized phase growth parameter S_A has been measured at point A or at the end of storage and prior to deployment. This damage parameter S_A was then mapped back on the thermal cycling curve (marked by point B) that corresponds to S_B to find the equivalent number of cycles N_B. Points A and B are points on the thermal aging and thermal cycling curves, respectively, corresponding to identical values of the normalized phase-growth parameter, i.e., $S_A = S_B$. Mapped cyclic life, N_B, corresponding to t_A hours of thermal aging represents the reduction in thermal cycle reliability because of pre-conditioning at a high temperature.

Similar damage equivalency relationships have been derived from the IMC growth measurements under thermal cycling
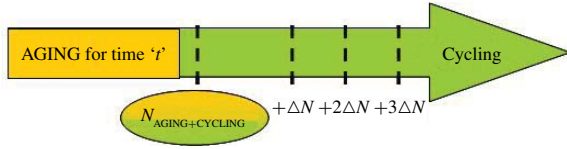
Fig. 7. Prognostication of AGED + THERMAL CYCLED sample at the same thermal cycle count $N1$.

and thermal aging. A normalized measure of microstructural evolution has been used in this case

$$\left(\frac{y_p}{y_0} - 1\right) = k_{N\Delta T} N^{n\Delta T} \qquad (8)$$

$$\left(\frac{y_p}{y_0} - 1\right) = k_{Nt} t^{nt}. \qquad (9)$$

Where y is the IMC thickness, subscripts p and 0 indicate point "p" and initial time, respectively, $k_{n\Delta T}$ and $n_{n\Delta T}$ are the normalized IMC growth coefficient and IMC growth exponent during thermal cycling, and k_{nt} and n_{nt} are the normalized IMC growth coefficient and IMC growth exponent during thermal aging. Convergence between the relationships has been used to validate that damage equivalency from thermal aging to thermal cycling reflects the underlying failure physics.

C. Validation of Damage Equivalency and Prognostication Under Overlapping Stresses

Test assemblies have been subjected to varying periods of thermal aging followed by thermal cycling. In each case, the assemblies subjected to known combinations of thermal aging and thermal cycling have been prognosticated based on the micro-structural evolution of damage. Prognostication involves withdrawal of four-samples from the deployed population of devices at four periodic intervals. The samples were then cross-sectioned and the damage proxies including phase-growth parameter and the IMC thickness was measured. Prior damage accrued was prognosticated. Normalized phase growth parameter was used to compute life consumed due to cycling alone

$$\frac{g_N^4}{g_0^4} - 1 = a_{N\Delta T}(N)^{b\Delta T} \qquad (10)$$

$$\frac{g_{N+\Delta N}^4}{g_0^4} - 1 = a_{N\Delta T}(N + \Delta N)^{b_{N\Delta T}} \qquad (11)$$

$$\frac{g_{N+2\Delta N}^4}{g_0^4} - 1 = a_{N\Delta T}(N + 2\Delta N)^{b_{N\Delta T}} \qquad (12)$$

$$\frac{g_{N+3\Delta N}^4}{g_0^4} = a_{N\Delta T}(N + 3\Delta N)^{b_{N\Delta T}}. \qquad (13)$$

The prognosticated damage was mapped using the damage equivalency relationships. Identical damage can be obtained by several combinations of thermal aging and thermal cycling. However, the use may be interested in particular solution relevant to the system of interest. The solution of the system of equations is thus bounded using t rust regions for range of acceptable values. Most operational systems have date-codes indicating the vintage of manufacture and deployment logs. This enables bounding of the analysis. The prognosticated value of accrued damage is represented by N_C. Reduction in cyclic life due to thermal aging is then be mapped to account for the storage time t_A prior to exposure to cycling. The mapped reduction in cyclic life is represented by N_B. The cyclic life is then

$$N_{\text{CYCLIC}} = N_C - N_B \qquad (14)$$

where N_{CYCLIC} is the life of the electronic system in thermal cycling. The RUL can then be calculated from the prognostic horizon.

IV. LM ALGORITHM

The relationship between the phase growth parameter and time is nonlinear because it contains terms with fourth power. Inverse solution for interrogation of system-state is challenging for damage evolution in such systems. LM algorithm n iterative technique that computes the minimum of a non-linear function in multi-dimensional variable space has been used for identifying the solution in the prognostication neighborhood [59]–[61]. Let f be a assumed functional relation between a measurement vector referred to as prior-damage and the damage parameter vector, p, referred to as predictor variables. The measurement vector is the current values of the leading-indicator of failure and the parameter vector includes the prior system state, and accumulated damage and the damage evolution parameters. An initial parameter estimate p_0 and a measured vector x are provided and it is desired to find the parameter vector p, that best satisfies the functional relation f i.e., minimizes the squared distance or squared-error, $\varepsilon^T \varepsilon$ with $\varepsilon = x - f(p)$. Assume that $g(p) = \varepsilon$ in the squared error. The minimizer parameter vector, p, for the error function has been represented as

$$F(p) = \frac{1}{2} \sum_{i=1}^{m} (g_i(p))^2 = \frac{1}{2} g(p)^T g(p) \qquad (15)$$

$$F'(p) = J(p)^T g(p) \qquad (16)$$

$$F''(p) = J(p)^T J(p) + \sum_{i=1}^{m} g_i(x) \, g_i'(x) \qquad (17)$$

where $F(p)$ represents the objective function for the squared error term $\varepsilon^T \varepsilon$, $J(p)$ is the Jacobian, and $F'(p)$ is the gradient, and $F''(p)$ is the Hessian. The variation of an F-value starting at "p" and with direction "h" is expressed as a Taylor expansion, as follows:

$$F(p + \alpha h) = F(p) + \alpha h^T F'(p) + O(\alpha^2) \qquad (18)$$

where α is the step-length from point "p" in the descent direction, "h." Mathematically, "h" is the descent direction of $F(p)$ if $h^T F'(p) < 0$. If no such "h" exists, then $F'(p) = 0$, showing that in this case the function is stationary. Since the condition for the stationary value of the objective function is that the gradient is zero, i.e., $f'(p + h) = L'(h) = 0$. The descent direction can be computed from the equation

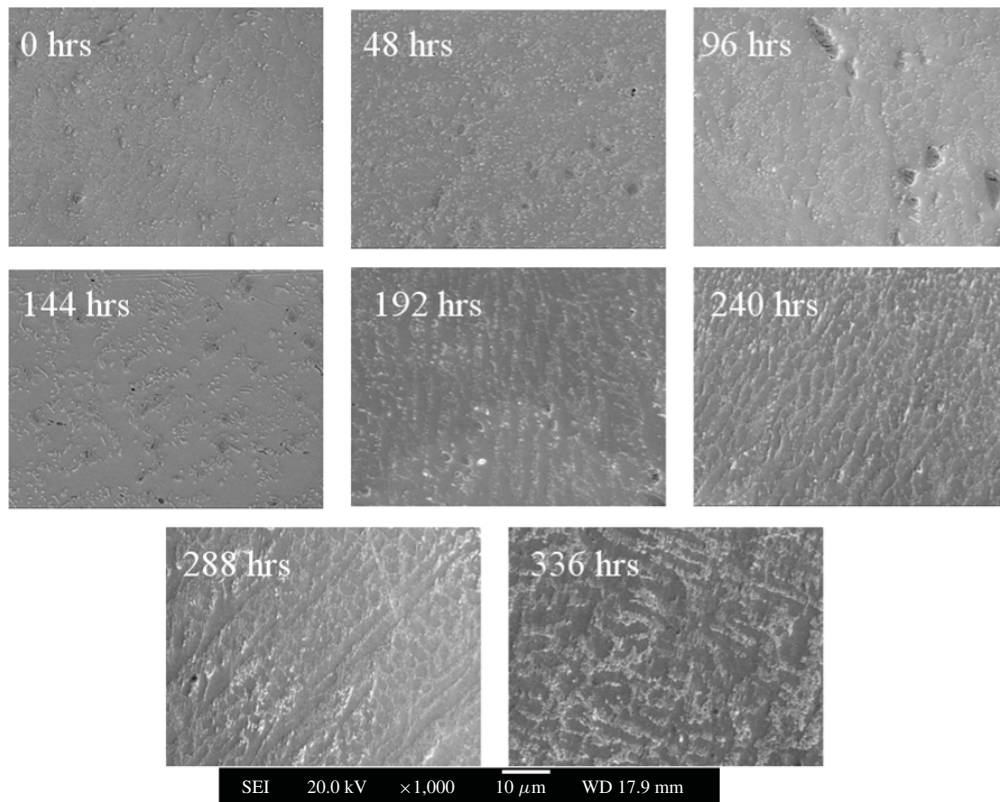$$\left(J^T J\right) h_{gn} = -J^T g. \qquad (19)$$

Fig. 8. SEM backscattered image of phase growth versus different aging time intervals (thermal aging at 125 °C, 96.5Sn3Ag0.5Cu solder, 676 I/O PBGA, magnification 750×).
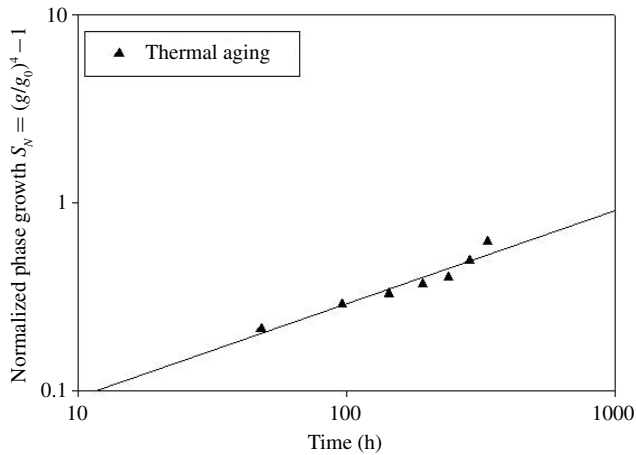

Fig. 9. Plot of normalized phase growth versus thermal aging time for 96.5Sn3.0Ag0.5Cu solder, 676 PBGA, subjected to thermal aging at 125 °C.

In each step, Newton method uses $\alpha = 1$, and $p = p + \alpha h_{gn}$, where subscript '*gn*' indicates Gauss–Newton. The value of α is found by line search principle described above. LM algorithm is a hybrid method which utilizes both steepest descent principle as well as the Gauss–Newton method. When the current solution is far from the correct one, the algorithm behaves like a steepest descent method: slow, but guaranteed to converge. When the current solution is close to the correct solution, it becomes a Gauss–Newton method. The LM method actually solves a slight variation of (25), known as the

augmented normal equations

$$\left(J^T J + \mu I\right) h = -J^T g. \tag{20}$$

The term μ is called as the damping parameter, $\mu > 0$ ensures that coefficient matrix is positive definite, and this ensures that h is a descent direction. When the value of μ is very small, then the step size for LM and Gauss–Newton are identical. Algorithm has been modified to take the equations of phase growth and IMC growth under both iso-thermal aging and cycling loads to calculate the unknowns.

V. CASE STUDY: PROGNOSTICATION OF DAMAGE IN LEADFREE AREA-ARRAY INTERCONNECTS UNDER SEQUENTIAL STRESSES

Samples subjected to single and sequential stresses have been prognosticated for damage equivalency and assessment of cumulative accrued damage resulting from a combination of thermal aging and thermal cycling. Prognosticated life has been correlated with experimental values. In addition, prognostic metrics have been computed to compare the robustness of the leading indicators and their accuracy in reference to the prognostic horizon.

A. Micro-Structural Evolution Under Thermal Aging

A set of packages was subjected to thermal aging at 125 °C and were withdrawn after each 48 h increment. The samples were cross-sectioned, polished. Phase growth and IMC growth
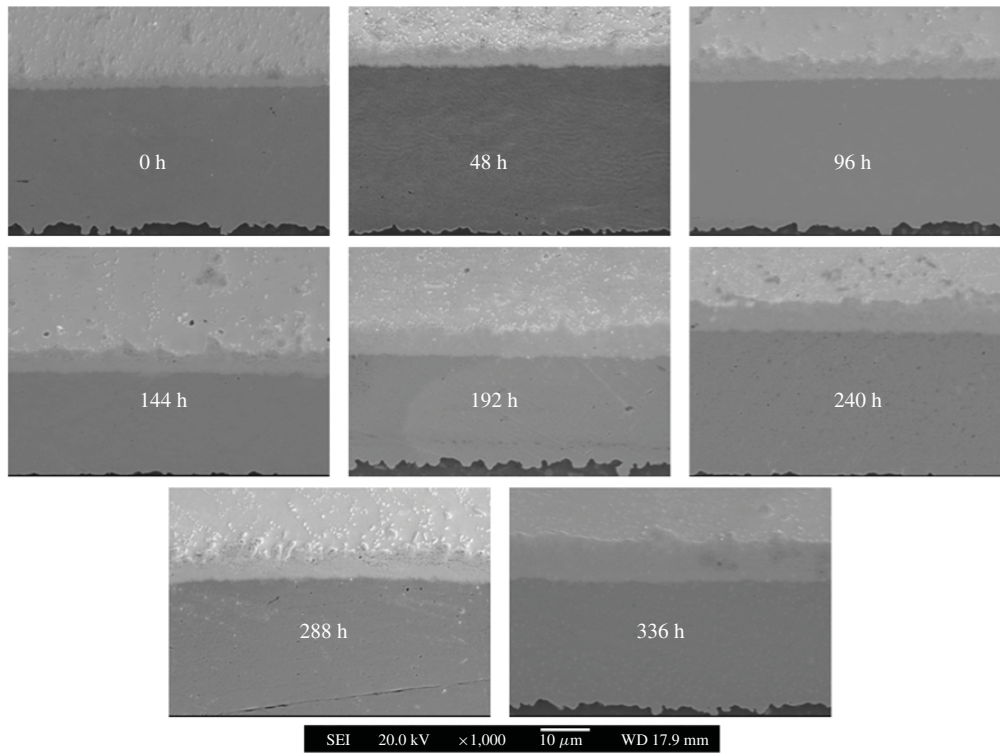
Fig. 10.   SEM backscattered image of IMC thickness versus different aging time intervals (thermal aging at 125 °C, 96.5Sn3.0Ag0.5Cu solder, 676 I/O PBGA, magnification 1000×).
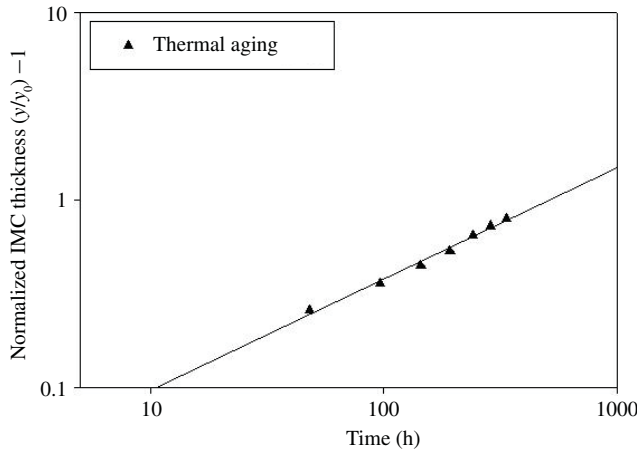

Fig. 11.   Plot of normalized IMC thickness versus aging time for 96.5Sn3.0Ag0.5Cu solder, 676 PBGA, subjected to thermal aging at 125 °C.

was studied using SEM images at each time intervals. The image analysis software has been used to measure the average phase size. Fig. 8 shows phase size at different aging time intervals and Fig. 9 shows the plot of normalized phase growth at various time intervals. The test data have been represented by the following equation:

$$S_{Nt} = \left(\frac{g_p}{g_0}\right)^4 - 1 = a_{nt} \, (t)^{b_{nt}} \tag{21}$$

where, g is the phase-growth, subscripts p and 0 indicate point "p" and initial time, respectively, S_{Nt} is the normalized phase-growth parameter during thermal aging, a_{nt} and b_{nt} are the normalized phase-growth coefficient and phase growth exponent for thermal aging. The following relationship

represents the evolution of phase-growth parameter in thermal aging based on experimental data. The equation parameters have been derived based on experimental measurements of the phase-growth parameters from cross-sections

$$S_N = 0.0297(t)^{0.49}. \tag{22}$$

Fig. 10 shows the growth of IMC thickness at various interval of time when subjected to thermal aging at 125 °C. Fig. 11 shows a plot of normalized IMC growth versus thermal aging time. The data have been fit to an equation for the following form:

$$\left(\frac{y_p}{y_0} - 1\right) = k_{Nt} t^{nt} \tag{23}$$

where y is the IMC thickness, subscripts p and 0 indicate point "p" and initial time, respectively, k_{nt} and n_{nt} are the normalized IMC growth coefficient and IMC growth exponent during thermal aging. The following relationship represents the evolution of IMC growth in thermal aging based on experimental data. The equation parameters have been derived based on experimental measurements of the IMC growth from cross-sections

$$\left[\frac{y}{y_0} - 1\right] = 0.044(t)^{0.5}. \tag{24}$$

B. Micro-Structural Evolution Under Thermal Cycling

A different set of assembly was subjected to thermal cycling from −55 °C to 125 °C and were withdrawn after each 100 cycle increments. The samples were cross-sectioned, polished. Phase growth and IMC growth was studied using SEM
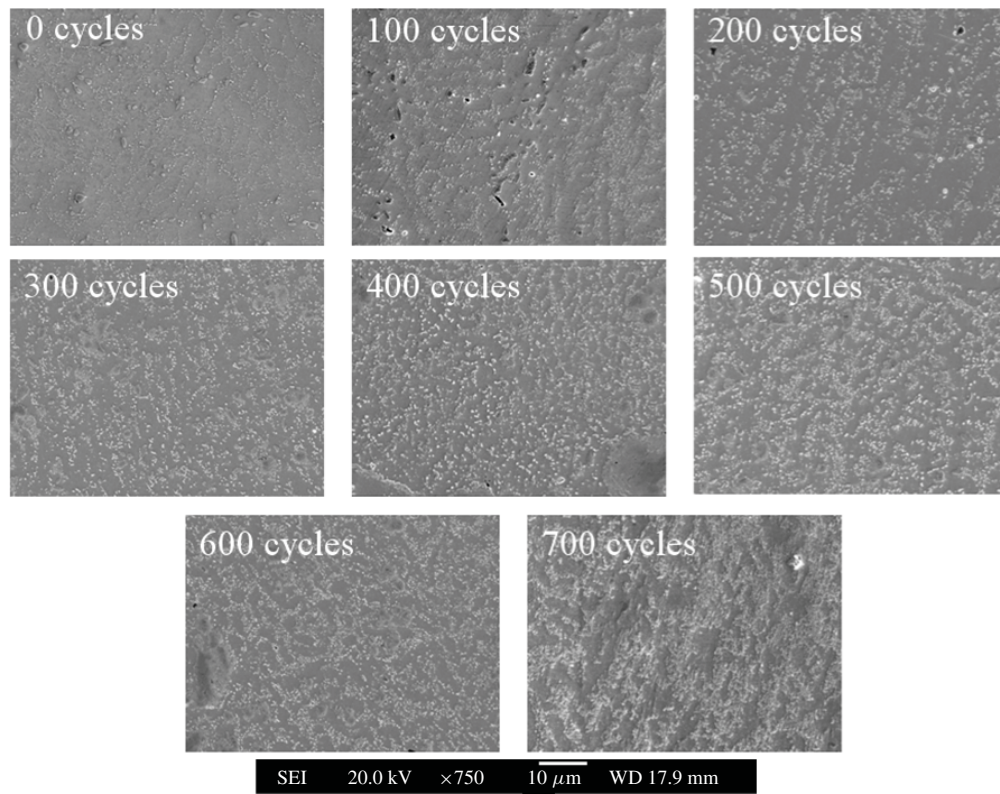
Fig. 12. SEM backscattered image of phase growth versus different aging time intervals (thermal cycling −55 °C to 125 °C, 96.5Sn3Ag0.5Cu solder, 676 I/O PBGA, magnification 750×).
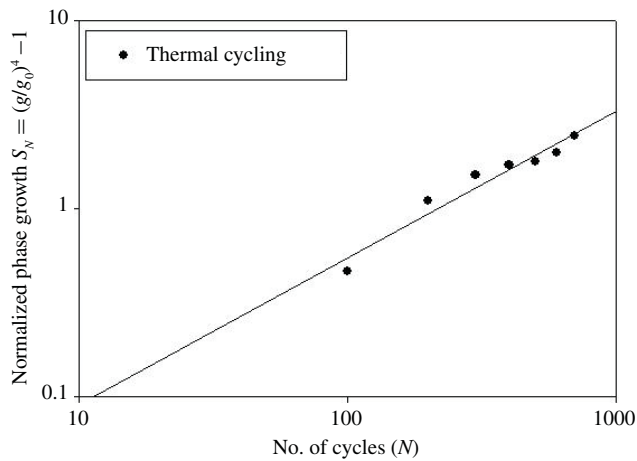

Fig. 13. Plot of normalized phase growth versus aging time for 96.5Sn3.0Ag0.5Cu Solder, 676 PBGA, subjected to thermal cycling from −55 °C to 125 °C.

images at each cyclic intervals. The image analysis software has been used to measure the average phase size. Fig. 12 shows phase size at different intervals of cycles and Fig. 13 shows the plot of normalized phase growth at various intervals of cycles. The test data have been fit to the following equation:

$$S_{N\Delta T} = \left(\frac{g_p}{g_0}\right)^4 - 1 = a_{n\Delta T} (N)^{b_{n\Delta T}} \qquad (25)$$

where g is the phase-growth, subscripts p and 0 indicate point "p" and initial time, respectively, $S_{N\Delta T}$ is the normalized

phase-growth parameter during thermal cycling, $a_{n\Delta T}$ and $b_{n\Delta T}$ are the normalized phase-growth coefficient and phase growth exponent during thermal cycling. The following relationship represents the evolution of phase-growth parameter in thermal cycling based on experimental data. The equation parameters have been derived based on experimental measurements of the phase-growth parameters from cross-sections

$$S_N = 0.015(N)^{0.78} \qquad (26)$$

where S_N is the normalized phase-growth parameter, and N is the number of cycles. Fig. 14 shows the growth of IMC thickness at various interval of time when subjected to thermal cycling from −55 to 125 °C. Fig. 15 shows a plot of normalized IMC growth versus thermal cycles. The data have been fit to an equation for the following form:

$$\left(\frac{y_p}{y_0} - 1\right) = k_{N\Delta T} N^{n\Delta T} \qquad (27)$$

where y is the IMC thickness, subscripts p and 0 indicate point "p" and initial time, respectively, $k_{n\Delta T}$ and $n_{n\Delta T}$ are the normalized IMC growth coefficient and IMC growth exponent during thermal cycling. The following relationship represents the evolution of IMC growth in thermal cycling based on experimental data. The equation parameters have been derived based on experimental measurements of the IMC growth from cross-sections

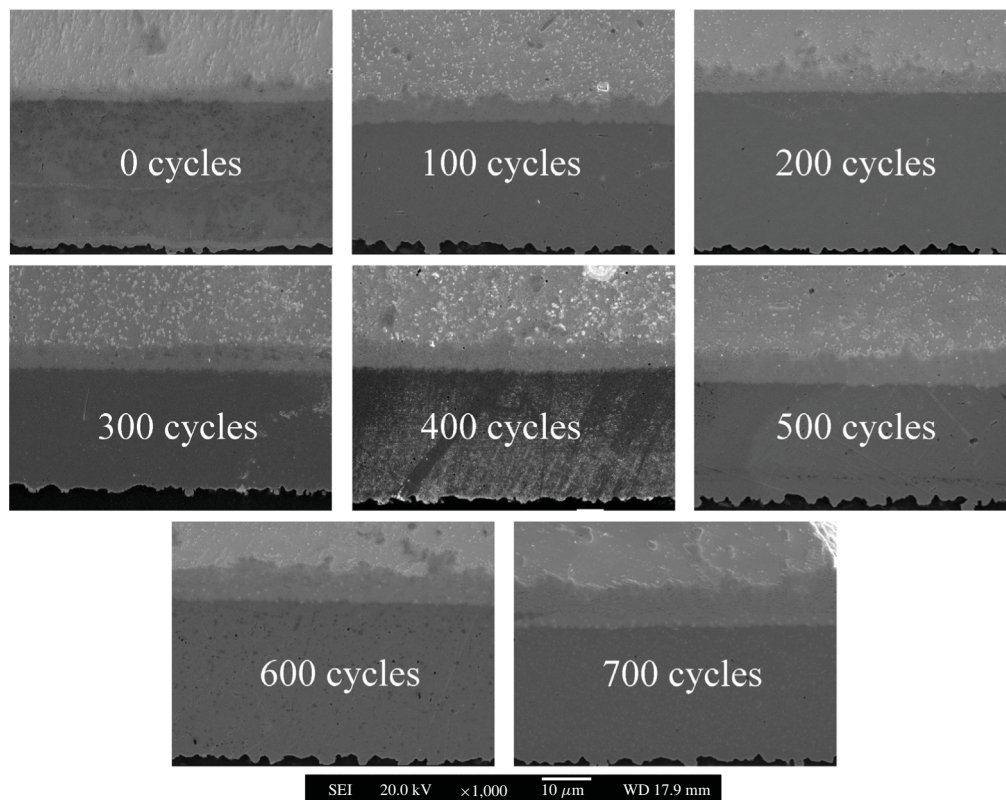$$\left[\frac{y}{y_0} - 1\right] = 0.0199(N)^{0.81}. \qquad (28)$$

Fig. 14.   SEM backscattered image of IMC thickness versus different aging time intervals (thermal cycling at −55 to 125 °C, 96.5Sn3.0Ag0.5Cu solder, 676 I/O PBGA, magnification 1000×).
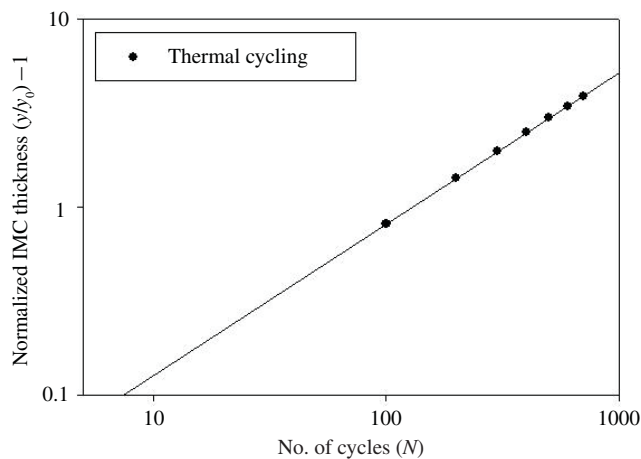

Fig. 15.   Plot of normalized IMC thickness versus no of cycles for 96.5Sn3.0Ag0.5Cu solder, 676 PBGA, subjected to thermal cycles from −55 °C to 125 °C.
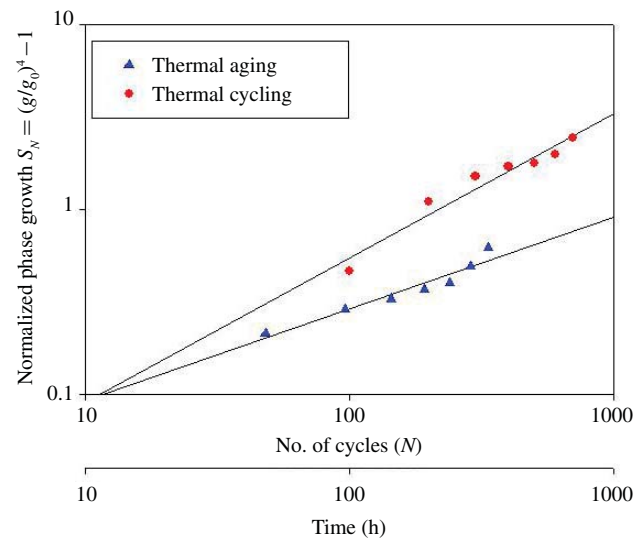
Fig. 16.   Combined plot normalized phase growth versus thermal aging time/thermal cycling.

C. Damage Equivalency Relationships Between Thermal Aging and Thermal-Cycling

Fig. 16 shows the combined plot normalized phase growth versus time and cycles on x-axis. Damage accrued from aging and cycling environments has been equivalenced based on two damage proxies including normalized IMC thickness and normalized phase growth. The evolution of normalized phase growth has been plotted versus thermal cycles in −55 to 125 °C and thermal aging time at 125 °C (Fig. 16). A similar value of damage proxy can be obtained by exposure to single stresses of thermal aging and thermal cycling. The exposure length to the environmental stresses, however, will be different in each case. This combined plot is helpful for mapping of damage from thermal aging onto thermal cycling.

Phase-growth parameter has been used for damage equivalency using previously derived equations for evolution of

Fig. 17. Combined plot of normalized IMC thickness versus thermal aging time/thermal cycling.

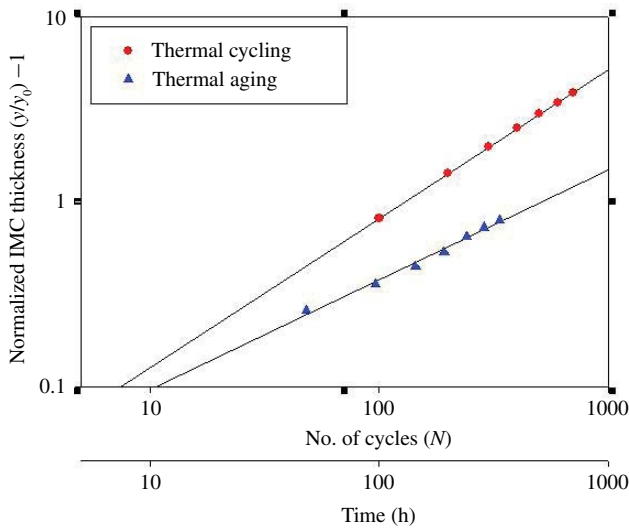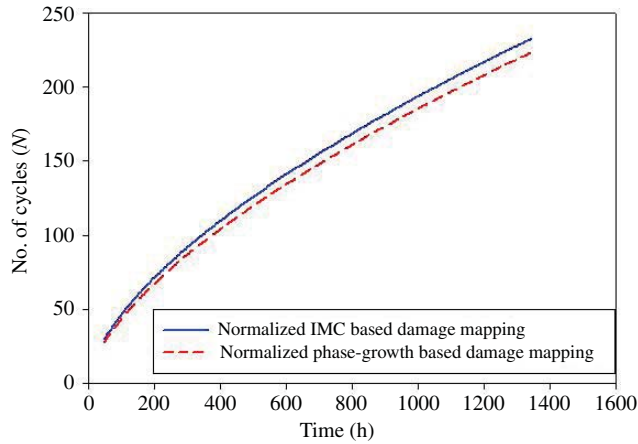Fig. 18. Combine plot of No of cycles (N) versus time in h, due to damage mapping from phase growth and IMC thickness.

S_N versus thermal aging time and thermal cycles. Equations (22) and (26) have been equated to derive the damage equivalence relationships based on phase-growth parameter

$$0.015(N)^{0.78} = 0.0297(t)^{0.49} \qquad (29)$$

$$N = 2.40(t)^{0.63} \qquad (30)$$

where N is the number of thermal cycles at -55 to $125\ ^\circ$C and t is the time in hours at $125\ ^\circ$C. Damage equivalency has also been studied using the IMC growth in second-level interconnects. The evolution of normalized IMC growth has been plotted versus thermal cycles in -55 to $125\ ^\circ$C and thermal aging time at $125\ ^\circ$C (Fig. 17). A similar value of IMC thickness can be obtained by exposure to single stresses of thermal aging and thermal cycling. The exposure length to the environmental stresses, however, will be different in each case. This combined plot is helpful for mapping of damage from thermal aging onto thermal cycling. Equations (24) and (28) have been equated to develop the damage equivalence

TABLE II
DAMAGE MAPPING FROM LEADING INDICATORS OF FAILURE

Time in h	Reduction in life from normalized phase parameter	Reduction in life from normalized IMC parameter
48	28	29
96	43	45
144	55	58
192	67	69
240	77	80
288	86	89
336	93	98

TABLE III
ERROR ESTIMATION IN PROGNOSTICATION OF THERMAL AGING

Life consumed	Cycle count		
	Expt	LM	%Error
48 h aging	48	46	4.2
192 h aging	192	178	7.3

relationships based on IMC growth

$$0.0199(N)^{0.81} = 0.044(t)^{0.5} \qquad (31)$$

$$N = 2.675(t)^{0.62}. \qquad (32)$$

Comparison of the damage equivalency relationships between thermal aging at $125\ ^\circ$C and thermal cycling from -55 to $125\ ^\circ$C developed based on the phase-growth parameter shows that both equations have similar coefficients and exponents (30), (32). The values on the graph and the table have been plotted and shown, respectively. The convergence of the damage equivalency parameters from two separate damage proxies bolsters the validity of the correlation. Fig. 18 and Table II shows the reduction in thermo-mechanical fatigue life derived based on the two damage proxies.

D. Prognostication of Damage Under Overlapping Stresses

Test assemblies have been exposed to overlapping sequential stresses of thermal aging at $125\ ^\circ$C and thermal cycling from -55 to $125\ ^\circ$C. Both the steady-state exposure and cyclic-thermal exposure has been done for various lengths for multiple sets of test assemblies. The system state has been interrogated using both the damage proxies discussed in this paper including phase-growth parameter and IMC growth. Samples have been withdrawn at periodic intervals and x-sectioned for measurement of the damage proxies. The LM-Algorithm has been used for interrogation of system-state for accrued damage. Fig. 19 shows the prognosticated value of 46 hours of thermal aging exposure for samples previously subjected to 48 hours of thermal aging. The prognosticated value of damage accrued correlates well with the actual value. Based on (30), it can be calculated that 46 hours in thermal aging at $125\ ^\circ$C maps to 26 cycles of reduction in life at -55 to $125\ ^\circ$C for the part tested. Thus, cyclic life will be reduced by 27 cycles due to thermal aging exposure of the assembly to 46 hours of $125\ ^\circ$C. Table IV summarizes the reduction in life and corresponding life in cyclic environment
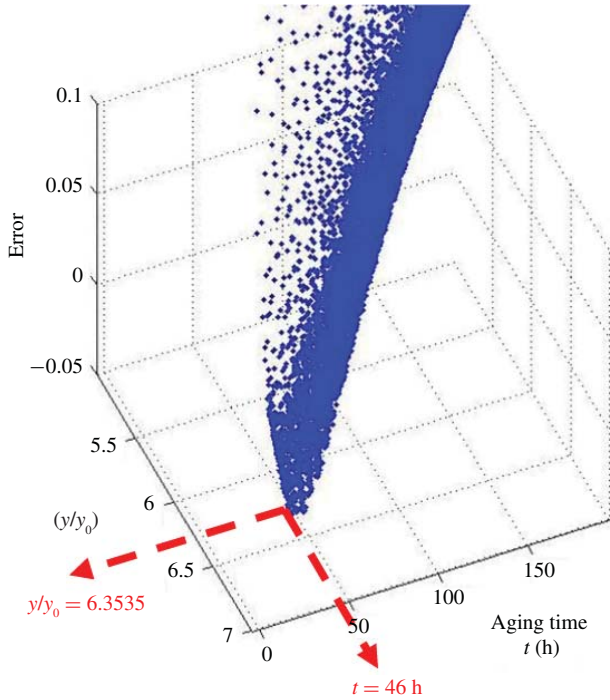
Fig. 19. 3-D plot of error versus aging time in h for 676 PBGA 96.5Sn3.0Ag0.5Cu solder interconnects for 48 h in thermal aging at 125 °C.

for two different aging intervals. The correlation between the experimental and prognosticated values is shown in Columns (A) and (B). Table V shows the correlation between assessments of damage accrued under overlapping thermal aging and thermal cycling for two conditions to (48 hours + 100 cycles) and (192 h + 100 cycles). Fig. 20 shows the prognostication output for the total life consumption due to storage and cyclic environment i.e., 48 h in aging followed by 100 cycles in cyclic environment. The prognosticated value of 143 cycles assumes cycling alone. Since the part was subjected to thermal aging followed by cycling, the actual value of cyclic life is $N_{CYCLIC} = 143 - 27 = 116$ Cycles. The prognosticated value of 116 cycles correlates well with 100 cycles of actual life. Similar process of prognostication of assemblies under overlapping stresses has been repeated for 192 hours of thermal aging at 125 °C followed by 100 cycles of thermal cycling from −55 to 125 °C. Similarly Figs. 21 and 22 show the prognostication results for 192 h of aging followed by cyclic exposure. Prognosticated life of 117 cycles correlates well with actual cyclic life of 100 cycles. The error in both cases is in the neighborhood of 8–12%.

VI. PROGNOSTICS PERFORMANCE METRICS

Prognostic metrics have been used to compare the robustness of the prognostication algorithms using these leading indicators of damage for overlapping sequential stresses of thermal aging and thermal cycling. The prognostics metrics used in this paper include: accuracy, precision, mean squared error (MSE), and mean absolute percentage error (MAPE), $\alpha - \lambda$ accuracy, relative accuracy (RA), and cumulative relative accuracy (CRA) have been computed to compare the two models [2], [3].

TABLE IV
ERROR ESTIMATION IN DAMAGE EQUIVALENCY OF THERMAL AGING

Aging time, t (h)	Reduction in life (cycles) $N = 2.40(t)^{0.63}$ (30) (A)	Prognosticated aging time, t (h)	Reduction in life (cycles) $N = 2.40(t)^{0.63}$ (30) (B)
48	28	46	27
192	66	178	63

Average Bias: The average bias method averages the error in predictions made at all subsequent times after prediction starts for the lth unit under test (UUT). The metric can be extended to average bias over all UUTs to establish overall bias [2], [3]

$$B_l = \frac{\sum_{i=P}^{EOP} \left\{ \Delta^l(i) \right\}}{(EOP - P + 1)} \quad (33)$$

where, end-of-prediction (EOP) is the earliest time index, i, after prediction crosses the failure threshold, P is the time index at which the first prediction is made by the prognostic system, $\Delta^l(i)$ is the error between the predicted and the true RUL at time index i for UUT l.

Sample Standard Deviation (S): The sample standard deviation measures the dispersion of the error with respect to the sample mean of the error. This metric is restricted to the assumption of normal distribution of error [2], [3]

$$S(i) = \sqrt{\frac{\sum_{l=1}^{n} \left(\Delta^l(i) - M \right)^2}{n - 1}} \quad (34)$$

where, M is sample mean of the error, and $\Delta^l(i)$ is the error between the predicted and the true RUL at time index i for UUT l.

MSE: The MSE averages the square prediction error for multiple UUTs at the same prediction horizon. A derivative of MSE is root MSE [2], [3]

$$MSE(i) = \frac{1}{L} \sum_{i=1}^{L} \Delta^l(i)^2 \quad (35)$$

where, $\Delta^l(i)$ is the error between the predicted and the true RUL at time index i for UUT l.

A. MAPE

MAPE averages the absolute error in the predictions of multiple UUTs at the same prediction horizon. Instead of the mean, median can be used to compute MAPE in similar fashion [2], [3]

$$MAPE(i) = \frac{1}{L} \sum_{l=1}^{L} \left| \frac{100 \Delta^l(i)}{r_*^l(i)} \right| \quad (36)$$

where, $r_*^l(i)$ is the true RUL at time t_i given that data is available up to time t_i for the lth UUT.

$\alpha - \lambda$ Accuracy: The $\alpha - \lambda$ curve has been plotted for both the models as shown in Figs. 23 and 24. It is a normalized plot

TABLE V
ERROR ESTIMATION IN PROGNOSTICATION OF OVERLAPPING DAMAGE

Stress history	Experiment			Prognostication			
	Life Reduction due to Aging (Cycles). Column A, Table III, (V)	Imposed Thermal Cycles (Cycles), (W)	Cyclic Life (Cycles) (V + W)	Prognosticated Life (Cycles), (X)	Life Reduction in due to Aging, (Cycles) Column B, Table III, (Y)	Cyclic Life Consumed (Cycles), (X–Y)	Error (%), (V + W) and (X)
48 h + 100 cyc	28	100	128	143	27	116	−11.7
192 h + 100 cyc	66	100	166	180	63	117	−8.4

3-D plot for prognostication of life consumed due to storage (t_A)

Fig. 21.   3-D plot of error versus aging time in h for 676 PBGA 96.5Sn3.0Ag0.5Cu solder interconnects for 192 h in thermal aging at 125 °C.

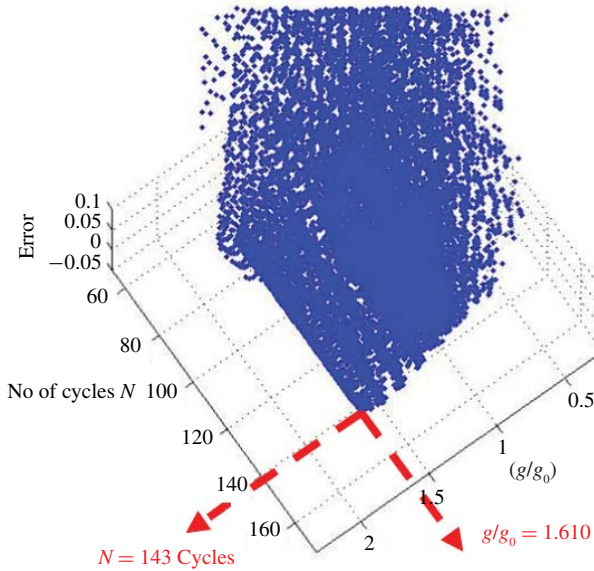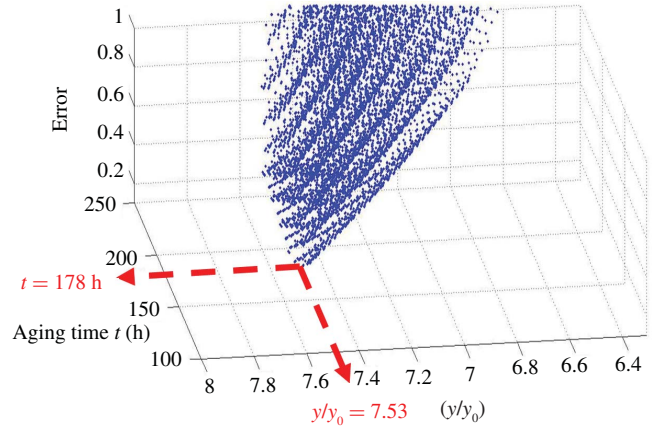3-D plot for prognostication of aging + cycling (N_2)

Fig. 20.   3-D plot of error versus number of cycles, life computed from LM-algorithm for 48 h in aging + 100 cycles in cycling environment for 676 PBGA 96.5Sn3.0Ag0.5Cu solder interconnects.

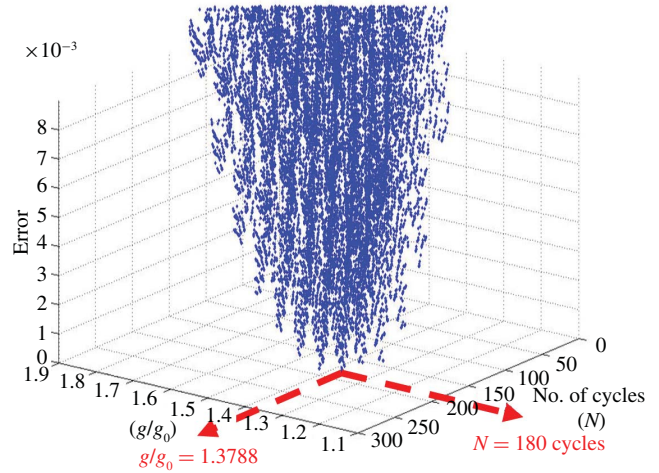3-D plot for prognostication of aging + cycling (N_2)

Fig. 22.   3-D plot of error versus prognosticated life for 192h in aging + 100 cycles in cycling environment for 676 PBGA 96.5Sn3.0Ag0.5Cu solder interconnects.

of RUL versus life which is compared against failure data and the error bounds. A value of 100% on the x-axis indicates that all the life has been consumed and the percentage RUL is zero. In this case, the experimental data obtained from accelerated testing shown by blue line in the plots and ±10% error bounds are shown by dotted lines. It should be noted that the selection of error bounds is application specific and typically tighter bounds are imposed as the criticality of the system increases. In this paper, the main idea to plot $\alpha - \lambda$ curves for the two models was not to find the prognostic horizon point but to compare the relative performance of the models visually. Both leading indicators perform well.

RA: The relative prediction accuracy has been used to asses whether the predictions fall within a given accuracy levels at a given time instant. The time instant is the fraction of actual RUL from the point when the first prediction is made. An algorithm with higher RA is desirable [2], [3]

$$\text{RA} = 1 - \frac{\left| r_*(t_\lambda) - r^l(t_\lambda) \right|}{r_*(t_\lambda)} \tag{37}$$

where $t_\lambda = P + \lambda \,(\text{EOP} - P)$, $r^l(i)$ is the RUL estimate for the lth UUT at time t_i as determined from measurement and analysis, $r_*^l(i)$ is the true RUL at time t_i given that data are available up to time t_i for the lth UUT.

CRA: RA has been evaluated at multiple time instances. CRA has been calculated as the normalized weighted sum of relative prediction accuracies at specific time instances

TABLE VI
COMPARISON OF PROGNOSTICS METRICS FOR THE TWO
LEADING INDICATORS

Prognostic metrics	LM prognostication (phase)	LM prognostication (IMC)
Average bias	−0.8232	2.2256
SSD (S)	220.61	292.89
MSE	54181	130216
MAPE	0.0658	0.1773
RA ($\lambda = 0.5$)	0.9732	0.7836
CRA	0.0077	0.0074

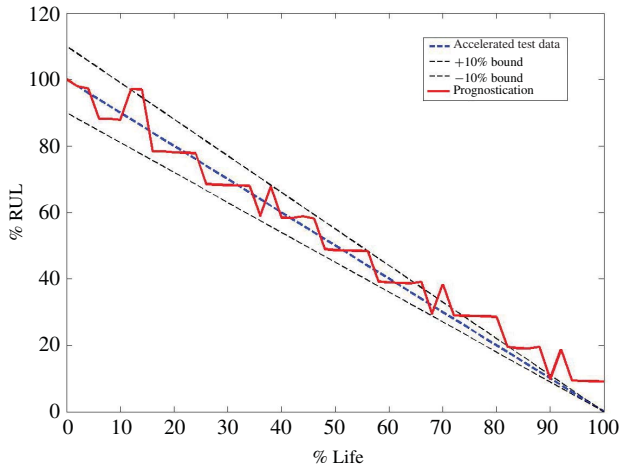Alpha-lambda curve for prognostication using phase-growth as the damage proxy

Fig. 23. $\alpha - \lambda$ curve for prognostication using phase-growth as the damage proxy.

[2], [3]

$$\text{CRA} = \frac{1}{\text{EOP} - P + 1} \sum_{l=P}^{\text{EOL}} \text{RA} \qquad (38)$$

where EOL represents end-of-life, w is a weight factor as a function of RUL at all time indices. In most cases it is desirable to weigh the RAs higher closer to the EOL. Table VI shows the RA for a point where 50% of the life of system is consumed. Both leading indicator based prognostic algorithms show comparable performance.

VII. DISCUSSION

The PHM technique presented in this paper may be implemented using condition monitoring devices, which can be cross-sectioned to interrogate the system state and determine the failure progression of the assembly. Consider an electronic assembly which has been deployed in the field applications. The assembly needs to be redeployed in the same environment. Interrogation of system state and prognostication of RUL may be implemented based on micro-structural evolution of damage assessed from cross-sections of system state sensor cells. The condition monitoring devices in the system will be withdrawn at periodic intervals in the deployed environment. The length of the periodic intervals does not effect implementation of the technique. The length of the periodic interval can be user defined. Prognostication will not add to downtime because

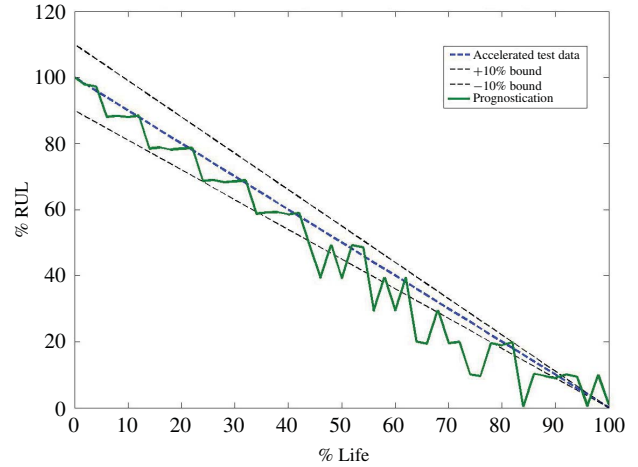Alpha-lambda curve for prognostication using IMC as the damage proxy

Fig. 24. $\alpha - \lambda$ curve for prognostication using IMC as the damage proxy.

the sample from sensor cell bank can be withdrawn and the equipment can continue operation. The condition monitoring devices will be cross-sectioned and their phase size data will be extracted. This data will be analyzed using LM Algorithm and methodologies discussed earlier, to find out the initial grain size (g_0) and the prior time of deployment (N, or t) for which the component has been deployed. The guess values have been chosen to encompass a wide range of expected values. For example 'N' is the number of cycles, so it can be in the range of 0–5000 cycles. The upper extreme is chosen such that it is higher than the expected design life of the part being examined. Similar process has been followed for other variables. Typically higher upper bounds for the array require longer time period to solve. The range of guess values for all the variables was provided to the algorithm. The rate of change of phase growth parameter, (dS/dN), will be computed using the computed values of damage proxies or leading indicators-of-failure.

It is envisioned that the system-state sensor-cells will be small, low cost, such that several of these can be conveniently located on card assemblies in vicinity of the electronic system, to enable cross-sectioning. The primary-system will not be damaged or impacted in any way by the prognostication method proposed. The proposed method also enables application of methodology to aged systems, and extends the state-of-art of conventional reliability prediction models which are applicable to pristine systems. For example, in the case of solder interconnects, chip resistors may be included on the board assembly and serve as system-state sensor-cells, which can be periodically cross-sectioned. It is not required to assume that all the components mounted on the same board have the same exposure to environmental or operational stresses.

VIII. CONCLUSION

A method has been developed for prognostication of accrued prior damage in electronics subjected to overlapping sequential environments of thermal aging and thermal cycling. The presented approach uses the LM Algorithm in conjunction

with microstructural evolution of damage based leading indicator for estimating prior stress history. Specific damage proxies examined include the phase-growth indicator and the IMC thickness. The viability of the approach has been demonstrated for leadfree test assemblies subjected to thermal aging at 125 °C and redeployed in cyclic thermo-mechanical environment −55–125 °C. Damage equivalency relationships between thermal aging during storage life and the resulting reduction in thermo-mechanical reliability in cyclic thermal environments during field deployment has been derived and validated based on two damage proxies. Convergence of the damage mapping to a common solution from data based on the two separate leading indicators has been demonstrated. Assemblies subjected to sequential stresses have been prognosticated for accrued damage from sequential overlapping stresses of thermal aging and thermal cycling. Correlation between the prognosticated damage and the actual accrued damage demonstrates that the proposed approach can be used to assess damage accrued under overlapping thermo-mechanical stresses of thermal aging and thermal cycling. In addition, prognostics metrics have been used to quantitatively evaluate the performance of the prognostic algorithms using both the leading indicators. Results demonstrate that both damage proxies work well in estimating accrued damage and estimating residual life.

REFERENCES

[1] D. Jarrell, D. Sisk, and L. Bond, "Prognostics and condition based maintenance (CBM) a scientific crystal ball," in *Proc. Int. Congr. Adv. Nucl. Power Plants*, Jun. 2002, p. 194.

[2] A. Saxena, J. Celaya, B. Saha, S. Saha, and K. Goebel, "Evaluating algorithm performance metrics tailored for prognostics," in *Proc. IEEE Aerosp. Conf.*, Big Sky, MT, Mar. 2008, pp. 1–11.

[3] A. Saxena, J. Celaya, E. Balaban, K. Goebel, B. Saha, S. Saha, and M. Schwabacher, "Metrics for evaluating performance of prognostic techniques," in *Proc. Int. Conf. Prognost. Health Manage.*, Denver, CO, Oct. 2008, pp. 1–17.

[4] K. A. Marko, J. V. James, T. M. Feldkamp, C. V. Puskorius, J. A. Feldkamp, and D. Roller, "Applications of neural networks to the construction of 'virtual' sensors and model-based diagnostics," in *Proc. ISATA 29th Int. Symp. Autom. Technol. Autom.*, Jun. 1996, pp. 133–138.

[5] R. S. McCann and L. Spirkovska, "Human factors of integrated systems health management on next-generation spacecraft," in *Proc. 1st Int. Forum Integr. Syst. Health Eng. Manage. Aerosp.*, Napa, CA, Nov. 2005, pp. 1–18.

[6] J. R. Schauz, "Wavelet neural networks for EEG modeling and classification," Ph.D. thesis, Dept. Electr. Eng., Georgia Inst. Technology, Atlanta, 1996.

[7] J. Shiroishi, Y. Li, S. Liang, T. Kurfess, and S. Danyluk, "Bearing condition diagnostics via vibration and acoustic emission measurements," *Mech. Syst. Signal Process.*, vol. 11, no. 5, pp. 693–705, Sep. 1997.

[8] P. Lall, P. Choudhary, S. Gupte, and J. Suhling, "Health monitoring for damage initiation and progression during mechanical shock in electronic assemblies," *IEEE Trans. Comp. Packag. Technol.*, vol. 31, no. 1, pp. 173–183, Mar. 2008.

[9] P. Lall, D. Panchagade, Y. Liu, R. W. Johnson, and J. C. Suhling, "Models for reliability prediction of fine-pitch BGAs and CSPs in shock and drop-impact," in *Proc. 54th Electron. Comp. Technol. Conf.*, Las Vegas, NV, Jun. 2004, pp. 1296–1303.

[10] P. Lall, D. Panchagade, Y. Liu, R. W. Johnson, and J. C. Suhling, "Models for reliability prediction of fine-pitch BGAs and CSPs in shock and drop-impact," *IEEE Trans. Comp. Packag. Technol.*, vol. 29, no. 3, pp. 464–474, Sep. 2006.

[11] P. Lall, S. Gupte, P. Choudhary, and J. Suhling, "Solder-joint reliability in electronics under shock and vibration using explicit finite element sub-modeling," in *Proc. 56th Electron. Comp. Technol. Conf.*, San Diego, CA, May–Jun. 2006, pp. 428–435.

[12] P. Lall, M. Hande, C. Bhat, N. Islam, J. Suhling, and J. Lee, "Feature extraction and damage-precursors for prognostication of leadfree electronics," *Microelectron. Rel.*, vol. 47, pp. 1907–1920, Dec. 2007.

[13] P. Lall, N. Islam, P. Choudhary, and J. Suhling, "Prognostication and health monitoring of leaded and lead free electronic and MEMS packages in harsh environments," in *Proc. 55th Electron. Comp. Technol. Conf.*, Orlando, FL, Jun. 2005, pp. 1–9.

[14] P. Lall, N. Islam, K. Rahim, J. Suhling, and S. Gale, "Leading indicators-of-failure for prognosis of electronic and MEMS packaging," in *Proc. 54th Electron. Comp. Technol. Conf.*, vol. 2. Las Vegas, NV, Jun. 2004, pp. 1570–1578.

[15] P. Lall, D. Iyengar, S. Shantaram, R. Pandher, D. Panchagade, and J. Suhling, "Design envelopes and optical feature extraction techniques for survivability of SnAg leadfree packaging architectures under shock and vibration," in *Proc. 58th Electron. Comp. Technol. Conf.*, Orlando, FL, May 2008, pp. 1036–1047.

[16] P. Lall, D. Panchagade, P. Choudhary, J. Suhling, and S. Gupte, "Failure-envelope approach to modeling shock and vibration survivability of electronic and MEMS packaging," in *Proc. 55th Electron. Comp. Technol. Conf.*, Orlando, FL, Jun. 2005, pp. 480–490.

[17] P. Lall, S. Shantaran, A. Angral, and M. Kulkarni, "Explicit submodeling and digital image correlation based life-prediction of leadfree electronics under shock-impact," in *Proc. 59th Electron. Comp. Technol. Conf.*, San Diego, CA, May 2009, pp. 542–555.

[18] P. Lall. R. Lowe, and K. Goebel, "Resistance spectroscopy-based condition monitoring for prognostication of high reliability electronics under shock-impact," in *Proc. 59th Electron. Comp. Technol. Conf.*, San Diego, CA, May 2009, pp. 1245–1255.

[19] P. Lall, C. Bhat, M. Hande, V. More, R. Vaidya, P. Pandher, J. Suhling, and K. Goebel, "Interrogation of system state for damage assessment in lead-free electronics subjected to thermo-mechanical loads," in *Proc. 58th Electron. Comp. Technol. Conf.*, Orlando, FL, May 2008, pp. 918–929.

[20] P. Lall, M. Hande, C. Bhat, V. More, R. Vaidya, and J. Suhling, "Algorithms for prognostication of prior damage and residual life in lead-free electronics subjected to thermo-mechanical loads," in *Proc. 10th ITherm*, Orlando, FL, May 2008, pp. 638–651.

[21] P. Lall, M. Hande, N. Singh, J. Suhling, and J. Lee, "Feature extraction and damage data for prognostication of leaded and leadfree electronics," in *Proc. 56th Electron. Comp. Technol. Conf.*, San Diego, CA, May–Jun. 2006, pp. 718–727.

[22] P. Lall, N. Islam, K. Rahim, J. Suhling, and S. Gale, "Prognostics and health management of electronic packaging," *IEEE Trans. Comp. Packag. Technol.*, vol. 29, no. 3, pp. 666–677, Sep. 2006.

[23] P. Lall, M. Hande, C. Bhat, J. Suhling, and J. Lee, "Prognostics health monitoring (PHM) for prior-damage assessment in electronics equipment under thermo-mechanical loads," in *Proc. 57th Electron. Comp. Technol. Conf.*, Reno, NV, May–Jun. 2007, pp. 1097–1111.

[24] P. Lall, V. More, R. Vaidya, and K. Goebel, "Prognostication of latent damage and residual life in leadfree electronics subjected to multiple thermal-environments," in *Proc. 59th Electron. Comp. Technol. Conf.*, San Diego, CA, May 2009, pp. 1381–1392.

[25] P. Lall, D. Panchagade, Y. Liu, W. Johnson, and J. Suhling, "Smeared property models for shock-impact reliability of area-array packages," *ASME J. Electron. Packag.*, vol. 129, pp. 373–381, Dec. 2007.

[26] P. Lall, P. Choudhary, S. Gupte, and J. Suhling, "Health monitoring for damage initiation & progression during mechanical shock in electronic assemblies," in *Proc. 56th Electron. Comp. Technol. Conf.*, San Diego, CA, May–Jun. 2006, pp. 85–94.

[27] P. Lall, P. Gupta, D. Panchagade, and A. Angral, "Fault-mode classification for health monitoring of electronics subjected to drop and shock," in *Proc. 59th Electron. Comp. Technol. Conf.*, San Diego, CA, May 2009, pp. 668–681.

[28] P. Lall, S. Gupte, P. Choudhary, and J. Suhling, "Solder-joint reliability in electronics under shock and vibration using explicit finite element sub-modeling," *IEEE Trans. Electron. Packag. Manuf.*, vol. 30, no. 1, pp. 74–83, Jan. 2007.

[29] P. Lall, N. Islam, T. Shete, J. Evans, J. Suhling, and S. Gale, "Damage mechanics of electronics on metal-backed substrates in harsh environments," in *Proc. 54th Electron. Comp. Technol. Conf.*, vol. 1. Las Vegas, NV, Jun. 2004, pp. 704–711.

[30] P. Lall, N. Islam, T. Shete, J. Evans, J. Suhling, and S. Gale, "Damage mechanics of electronics on metal-backed substrates in harsh environments," *IEEE Trans. Comp. Packag. Technol.*, vol. 29, no. 1, pp. 204–212, Mar. 2006.

[31] P. Lall, D. Iyengar, S. S. Shantaram, P. Gupta, D. Panchagade, and J. Suhling, "Keynote Presentation: Feature extraction and health monitoring using image correlation for survivability of leadfree packaging under shock and vibration," in *Proc. EuroSIME*, Freiburg, Germany, Apr. 2008, pp. 594–608.

[32] P. Lall, N. Islam, J. C. Suhling, and R. Darveaux, "Model for BGA and CSP reliability in automotive underhood applications," *IEEE Trans. Comp. Packag. Technol.*, vol. 27, no. 3, pp. 585–593, Sep. 2004.

[33] P. Lall, D. Panchagade, P. Choudhary, S. Gupte, and J. Suhling, "Failure-envelope approach to modeling shock and vibration survivability of electronic and MEMS packaging," *IEEE Trans. Comp. Packag. Technol.*, vol. 31, no. 1, pp. 104–113, Mar. 2008.

[34] P. Lall, P. Choudhary, S. Gupte, J. Suhling, and J. Hofmeister, "Statistical pattern recognition and built-in reliability test for feature extraction and health monitoring of electronics under shock loads," in *Proc. 57th Electron. Comp. Technol. Conf.*, Reno, NV, May–Jun. 2007, pp. 1161–1178.

[35] Y. Zhang, Z. Cai, J. Suhling, P. Lall, and M. Bozack, "The effects of SAC alloy composition on aging resistance and reliability," in *Proc. 59th Electron. Comp. Technol. Conf.*, San Diego, CA, May 2009, pp. 370–389.

[36] R. Chandramouli and S. Pateras, "Testing systems on a chip," *IEEE Spectrum*, vol. 33, no. 11, pp. 42–47, Nov. 1996.

[37] R. Drees and N. Young, "Role of BIT in support system maintenance and availability," *IEEE Aerosp. Electron. Syst. Mag.*, vol. 19, no. 8, pp. 3–7, Aug. 2004.

[38] A. Hassan, V. K. Agarwal, B. Nadeau-Dostie, and J. Rajski, "BIST of PCB interconnects using boundary-scan architecture," *IEEE Trans. Comput.-Aid. Design*, vol. 11, no. 10, pp. 1278–1288, Oct. 1992.

[39] T. W. Williams and K. P. Parker, "Design for testability-survey," *Proc. IEEE*, vol. 71, no. 1, pp. 98–112, Jan. 1983.

[40] Y. Zorian, "A structured testability approach for multichip boards based on BIST and boundary scan," *IEEE Trans. Comp. Packag. Manuf. Technol. Part B*, vol. 17, no. 3, pp. 283–290, Aug. 1994.

[41] D. Allen, "Probabilities associated with a built-in-test system, focus on false alarms," in *Proc. AUTOTESTCON, IEEE Syst. Read. Technol. Conf.*, Sep. 2003, pp. 643–645.

[42] R. X. Gao and A. Suryavanshi, "BIT for intelligent system design and condition monitoring," *IEEE Trans. Instrum. Meas.*, vol. 51, no. 5, pp. 1061–1067, Oct. 2002.

[43] D. Rosenthal and B. Wadell, "Predicting and eliminating built-in test false alarms," *IEEE Trans. Rel.*, vol. 39, no. 4, pp. 500–505, Oct. 1990.

[44] N. Anderson and R. Wilcoxon, "Framework for prognostics of electronic systems," in *Proc. Int. Military Aerosp. Avion. COTS Conf.*, Seattle, WA, Aug. 2004, pp. 1–29.

[45] S. Mishra and M. Pecht, "In-situ sensors for product reliability monitoring," *Proc. SPIE*, vol. 4755, pp. 10–19, Apr. 2002.

[46] T. E. Munns and R. M. Kent, "Structural health monitoring: Degradation mechanism and system requirements," in *Proc. Digital Avion. Syst. Conf.*, vol. 2. 2000, pp. 6C2/1–6C2/8.

[47] C. Baldwin, J. Kiddy, T. Salter, P. Chen, and J. Niemczuk, "Fiber optic structural health monitoring system: Rough sea trials testing of the RV Triton," in *Proc. MTS/IEEE Oceans*, vol. 3. Oct. 2002, pp. 1807–1814.

[48] P. C. Chang, A. Flatau, and S. C. Liu, "Review paper: Health monitoring of civil infrastructure," *Struct. Health Monitor.*, vol. 2, no. 3, pp. 257–267, 2003.

[49] L. Frosini and E. Bassi, "Stator current and motor efficiency as indicators for different types of bearing faults in induction motors," *IEEE Trans. Ind. Electron.*, vol. 57, no. 1, pp. 244–251, Jan. 2010.

[50] B. Lu and V. Gungor, "Online and remote motor energy monitoring and fault diagnostics using wireless sensor networks," *IEEE Trans. Ind. Electron.*, vol. 56, no. 11, pp. 4651–4659, Nov. 2009.

[51] R. Romary, S. Jelassi, and J. F. Brudny, "Stator-interlaminar-fault detection using an external-flux-density sensor," *IEEE Trans. Ind. Electron.*, vol. 57, no. 1, pp. 237–243, Jan. 2010.

[52] Y. Xiong, X. Cheng, Z. Shen, C. Mi, H. Wu, and V. Garg, "Prognostic and warning system for power-electronic modules in electric, hybrid electric, and fuel-cell vehicles," *IEEE Trans. Ind. Electron.*, vol. 55, no. 6, pp. 2268–2276, Jun. 2008.

[53] A. Y. Goharrizi and N. Sepehri, "A wavelet-based approach to internal seal damage diagnosis in hydraulic actuators," *IEEE Trans. Ind. Electron.*, vol. 57, no. 5, pp. 1755–1763, May 2010.

[54] D. Barke and W. K. Chiu, "Structural health monitoring in the railway industry: A review," *Struct. Health Monitor.*, vol. 4, no. 1, pp. 81–93, 2005.

[55] S. Bader, W. Gust, and H. Hieber, "Rapid formation of intermetallic compounds by interdiffusion in the Cu-Sn and Ni-Sn systems," *Acta Metall. Mater.*, vol. 4, no. 1, pp. 329–337, 1995.

[56] G. Y. Li and B. L. Chen, "Formation and growth kinetics of interfacial intermetallics in Pb-free solder joint," *IEEE Trans. Comp. Packag. Technol.*, vol. 26, no. 3, pp. 651–658, Sep. 2003.

[57] A. C. So and Y. C. Chan, "Reliability studies of surface mount solder joints - effect of Cu-Sn intermetallic compounds," *IEEE Trans. Comp. Packag. Manuf. Technol. B*, vol. 19, no. 3, pp. 661–668, Aug. 1996.

[58] Y. Wu, J. A. Sees, C. Pouraghabagher, L. A. Foster, J. L. Marchall, E. G. Jacobs, and R. F. Pinizzotto, "The formation and growth of intermetallics in composite solder," *J. Electron. Mater.*, vol. 22, no. 7, pp. 769–777, 1993.

[59] M. I. A. Lourakis, "A brief description of the Levenberg-Marquardt algorithm implemened by Levmar," *Found. Res. Technol.*, vol. 3, pp. 1–6, Feb. 2005.

[60] K. Madsen, H. B. Nielsen, and O. Tingleff, *Methods for Non-Linear Least Squares Problems*, 2nd ed. Copenhagen, Denmark: Technical University Denmark, 2004, pp. 1–30.

[61] H. B. Nielsen, "Damping parameter in Marquardt's method," Dept. Math. Modelling, Tech. Univ. Denmark, Copenhagen, Denmark, Tech. Rep. IMM-REP-1999-05, 1999, pp. 1–16.

Pradeep Lall (SM'08–F'12) received the B.E. degree in mechanical engineering from the Delhi College of Engineering, New Delhi, India, in 1988, the M.S. and Ph.D. degrees in mechanical engineering from the University of Maryland, College Park, in 1989 and 1993, respectively, and the M.B.A. degree from the Kellogg School of Management, Northwestern University, Evanston, IL, in 2002.

He is the Thomas Walter Professor with the Department of Mechanical Engineering and Director of the National Science Foundation Center for Advanced Vehicle and Extreme Environment Electronics, Auburn University, Auburn, AL. He has ten years of industry experience. He was previously with Motorola's Wireless Technology Center, Schaumburg, IL. He has published extensively in the area of electronic packaging with emphasis on modeling and predictive techniques. He is the author and co-author of two books, 13 book chapters, and over 270 journal and conference papers in the field of electronic packaging with emphasis on design, modeling, and predictive techniques. He holds three U.S. Patents.

Dr. Lall is a fellow of the American Society of Mechanical Engineers (ASME). He is a member of the National Academies Committee on Electronic Vehicle Controls and Unintended Acceleration. He is a member of the Beta Gamma Sigma Honorary Society. He is a recipient of the Samuel Ginn College of Engineering Senior Faculty Research Award and three-Motorola Outstanding Innovation Awards. He has received five Motorola Engineering Awards and four Publication Awards. He is a Six-Sigma Black-Belt in Statistics. He is the founding Faculty Advisor for the SMTA Student Chapter at Auburn University and a member of the Editorial Advisory Board for *SMTA Journal*. He is a member of the IEEE Reliability Society Advisory Committee. He is the Vice-Chair of the ASME Congress Steering Committee. He is an Associate Editor of the *ASME Journal of Electronic Packaging* and the IEEE TRANSACTIONS ON COMPONENTS AND PACKAGING TECHNOLOGIES.

Rahul Vaidya received the B.E. degree in electronics engineering from the University of Mumbai, Mumbai, India, in 2006. He received the M.S. degree from Auburn University, Auburn, AL.

He was a Graduate Research Assistant with the National Science Foundation Center for Advanced Vehicle and Extreme Environment Electronics, Department of Mechanical Engineering, Auburn University, under the guidance of Prof. P. Lall. His current research interests include prognostication of lead-free electronics subjected to thermo-mechanical loading.

Vikrant More received the B.E. degree in mechanical engineering from the University of Mumbai, Mumbai, India, in 2006, and the M.S. degree from Auburn University, Auburn, AL.

He was a Graduate Research Assistant with the National Science Foundation Center for Advanced Vehicle and Extreme Environment Electronics, Department of Mechanical Engineering, Auburn University, under the guidance of Prof. P. Lall. His current research interests include prognostics of electronic assemblies in cyclic thermo-mechanical environments.

Kai Goebel received the Diplom-Ingenieur degree from Technische Universität München, Munich, Germany, and the M.S. and Ph.D. degrees from the University of California, Berkeley, in 1990, 1993, and 1996, respectively.

He was with General Electric's Corporate Research Center, Niskayuna, NY, from 1997 to 2006, as a Senior Research Scientist. He has carried out applied research in the areas of artificial intelligence, soft computing, and information fusion. He is a Senior Scientist with NASA Ames Research Center, Moffett Field, CA, where he leads the Diagnostics and Prognostics Groups in the Intelligent Systems Division. In addition, he directs the Prognostics Center of Excellence and he is an Associate Principal Investigator for the Prognostics of NASA's Integrated Vehicle Health Management Program. He has published more than 150 papers in the area of systems health management and holds 11 patents. His current research interests include advancing these techniques for real time monitoring, diagnostics, and prognostics.